


Surface mines composite slope deformation mechanisms and stress distribution

Yamah J. Barvor¹✉, Sher Bacha^{1,2*} , Cai Qingxiang¹✉, Chen S. Zhao¹✉, Mohammad Siddique²✉

¹School of Mines, China University of Mining and Technology, Xuzhou, 221116, China

²Balochistan University of Information Technology, Engineering and Management Sciences, Quetta, 87300, Pakistan

*Corresponding author: e-mail enr_shahswati@yahoo.com, tel. +8615262008175

Abstract

Purpose. To analyze surface mines composite slope deformation mechanisms and stress distribution.

Methods. Description and interpretations of the mechanical and stress computational model for a waste dump loading in the formation of a composite slope on the basis of the theory of plasticity and elasticity. Numerical and analytical simulations for composite slope stress distribution.

Findings. From the numerical and analytical simulations, it is found that the increase in slope height and angle results in an increase in stress within the geo stress field of a composite slope. The numerical simulation also shows that as the dump is moved away from the point of application the settlement induced by the dump is larger beneath the dump and decreases away from the dump, hence the stress reduces. This highlights the sensitivity in simulating the effect of the waste dump at different position within the computation analysis of a composite slope stability problem. Furthermore, it is obtained that the stress induced by a trapezoidal loading is lesser than that of a rectangular loading, which is obvious. Finally, this paper provides the stress influence rule due to excavation in a surface mining operation. The stresses due to the dump loading were obtained and compared to stresses obtained from finite element analysis and both results are well in agreement.

Originality. The paper provides novel approach for the mechanisms of composite slope stress distribution and deformation mechanisms.

Practical implications. The results effectively describe the stress distribution mechanisms and stability analysis of composite slopes and provides basis for the preliminary design and stability of composite slopes.

Keywords: composite slope; deformation mechanism, waste dump, theory of plasticity

1. Introduction

The failure mechanism of composite slope is a complex phenomenon in that the removal of the overburden to recover the ore induces plastic and elastic deformation in the rock mass geometry and the construction of the waste dump near the mining limit induces additional stresses within the rock mass [1]-[4]. The distinction between the two forms of instabilities can be reduced to one of gravitational versus applied load [5], [6] and the incorporation of both failure mechanisms can be best suited to describe the instability mechanism governing a composite slope. The construction of composite slope may pose great challenges to the economic extraction of ores, protection of employees, equipment and safe production operation, if the lack of knowledge, limitation and understanding of the governing laws of stresses due to composite loading to that of creating an excavation in surface mining and the interactions amongst composite slope geometrical parameters are not well addressed [7]-[10]. Considering the smoothness of transporta-

tion flow, reduction in haul distance and lower transportation cost, the outer dump is generally located near the mining limit; however, the issue of validity of the concept for understanding the influence of the dump position and its interaction with key geometrical parameters of both the pit slope and the waste dump may lead to disastrous failures and landslide [11]-[13]. As a systematic and comprehensive study of the geometrical parameters of a composite slope, the need for understanding the influence of the dump position and the induced stress caused by loading and unloading is very important [4], [14]-[18]. It is possible only if the dump position, the induced stresses and the key geometrical parameters influences are clearly understood, that the ability to predict a composite slope failure mechanism could be developed which in return would lead to economic designs [19]-[26]. Two necessary steps that must then be taken to address this problem are the assessment of the primary factors influencing composite slope stability and the development of a clearer understanding of the failure modes and mechanisms involved.

2. Materials and methods

In the current study Datang Surface coal mine located within the eastern part of Shengli coalfield, a project of Datang international power generation co., LTD located in Xilingol league, Inner Mongolia autonomous region is used as a case study. Sigma/W Geo slope is used for the numerical and analytical simulation. Sigma/W is powerful finite element software for modeling stress and deformation in earth and structural materials. It analyses from simple linear elastic simulations to soil-structure interaction problems with nonlinear material models [27]. The Concept of finite element method is utilized. The relationship between loading conditions and slope parameters is analyzed using theory of plasticity and elasticity.

2.1. Two-dimensional stress state and slip lines analysis for composite slope

The stress structure derived for the composite slope is a plane strain two dimensional problem with three unknown components of stress (σ_{xx} , σ_{zz} , τ_{xz}) [28]. In a plane strain analysis, one dimension of the stress component is much greater than the other two dimensions. To begin our analysis, let's (x , z) represents the plane of unknown stress components such that the two-dimensional stress matrix is written in the form:

$$\begin{bmatrix} \sigma_{xx} & \tau_{xz} \\ \tau_{zx} & \sigma_{zz} \end{bmatrix}. \tag{1}$$

And the three components of stress obey the two-dimensional form of the equilibrium equations:

$$\begin{aligned} \frac{\partial \sigma_{xx}}{\partial x} + \frac{\partial \tau_{xz}}{\partial z} &= 0; \\ \frac{\partial \tau_{xz}}{\partial x} + \frac{\partial \sigma_{zz}}{\partial z} &= 0. \end{aligned} \tag{2}$$

Figure 1 shows a sketch of a Mohr circle and the two dimensional stress state where it has been assumed that σ_1 and σ_3 represents the principal stresses lying on the (x , z) plane and the intermediate stress σ_2 is normal to the plane and remains the intermediate principal stress no matter what happens to the other stresses. The stress points corresponding to (σ_{xx} , τ_{xz}) and (σ_{zz} , τ_{xz}) are plotted at arbitrary locations on the circle circumference except that they lie at the end of each diameter, and the pole of the Mohr circle is shown.

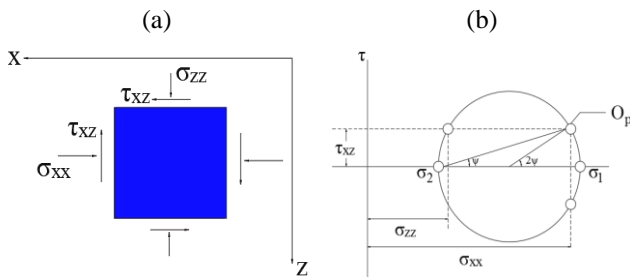


Figure 1. Mohr's diagram for a two-dimensional stress state [29]

From Figure 1, let ψ be the angle between the minor principal surface and the horizontal such that p represents the two dimensional mean stress defined as:

$$p = \frac{1}{2}(\sigma_{xx} + \sigma_{zz}) = \frac{1}{2}(\sigma_1 + \sigma_3). \tag{3}$$

The mean stress obtained in this analysis is completely different from the mean stress obtained in a three-dimensional stress state but it represents the average normal stress for a two-dimensional stress state, and it also identifies the location of the center of the Mohr's circle. If the angle ψ is introduced along with the radius of the circle the stress state at any point can be obtained. However, the only missing information is how the surfaces are oriented with regards to the (x , z) plane which leads to the introduction of slip lines as shown in Figure 2.

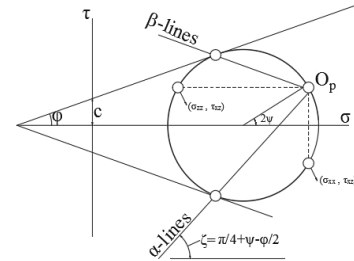


Figure 2. Mohr diagram for a slip line orientation [29]

Considering the Mohr circle shown in Figure 2, the radius of the circle is a function of the two-dimensional mean stress p according to:

$$\frac{1}{2}(\sigma_1 - \sigma_3) = \frac{1}{2} \left[(\sigma_{xx} - \sigma_{zz})^2 + 4\tau_{xz}^2 \right]^{\frac{1}{2}} = c \cos \varphi + p \sin \varphi. \tag{4}$$

It can be seen from Figure 2, that α - and β - lines intersect at an angle of $\pi/2 - \varphi$. Thus, the two dimensional mean stress p and angle ψ , can be fully characterize in order to state the two dimensional stress state as follows:

$$\begin{aligned} \sigma_{xx} &= p + (c \cos \varphi + p \sin \varphi) \cos 2\psi; \\ \sigma_{yy} &= p - (c \cos \varphi + p \sin \varphi) \cos 2\psi; \\ \tau_{xy} &= (c \cos \varphi + p \sin \varphi) \sin 2\psi. \end{aligned} \tag{5}$$

Using these equations to replace the stress components in the equilibrium Equations (2) gives:

$$\begin{aligned} (1 + \sin \varphi \cos 2\psi) \frac{\partial p}{\partial x} + \sin \varphi \sin 2\psi \frac{\partial p}{\partial y} &= \\ 2(c \cos \varphi + p \sin \varphi) \left(\sin 2\psi \frac{\partial \psi}{\partial x} - \cos 2\psi \frac{\partial \psi}{\partial y} \right); \\ \sin \varphi \sin 2\psi \frac{\partial p}{\partial x} + (1 - \sin \varphi \cos 2\psi) \frac{\partial p}{\partial x} &= \\ = -2(c \cos \varphi + p \sin \varphi) \left(\cos 2\psi \frac{\partial \psi}{\partial x} + \sin 2\psi \frac{\partial \psi}{\partial y} \right). \end{aligned} \tag{6}$$

If l_a represents the distance measured along α - line and the directional derivative of the mean stress p is taking then:

$$\frac{dp}{dl_a} = \frac{\partial p}{\partial x} \cdot \frac{dx}{dl_a} + \frac{\partial p}{\partial y} \cdot \frac{dy}{dl_a} = \frac{\partial p}{\partial x} \cos \omega + \frac{\partial p}{\partial y} \sin \omega. \tag{7}$$

Solving for $\frac{\partial p}{\partial x}$ and $\frac{\partial p}{\partial y}$ using (8) to find the equation of the α - line:

$$\frac{dp}{dl_a} = -2(c + p \tan \varphi) \frac{\partial \omega}{\partial l_a}. \tag{8}$$

A similar result applies for β -line with the sign on the right-hand side of the equation being reversed. Integrating gives:

$$\begin{aligned} \alpha\text{-line} &\rightarrow \ln(c + p \tan \varphi) + 2(\tan \varphi)\psi = C_1; \\ \beta\text{-line} &\rightarrow \ln(c + p \tan \varphi) - 2(\tan \varphi)\psi = C_2. \end{aligned} \tag{9}$$

Thus (9) can be used to relate the stress state along any characteristics line and everywhere on the characteristics line p and ψ are linearly related and if p and ψ are known the constant C_1 and C_2 can be obtained. Hence the stress variation beneath the waste dump can be obtained. The outer dump resting on the surface mines slope can be represented as a uniform traction that is applied on a surface of a homogeneous half space and different α - and β -lines can be drawn for the failure surfaces beneath the dump. Considering the proposed composite slope stress structure shown in Figure 3, Mohr circles for the three failure surfaces beneath the dump can be represented as those shown in Figure 4.

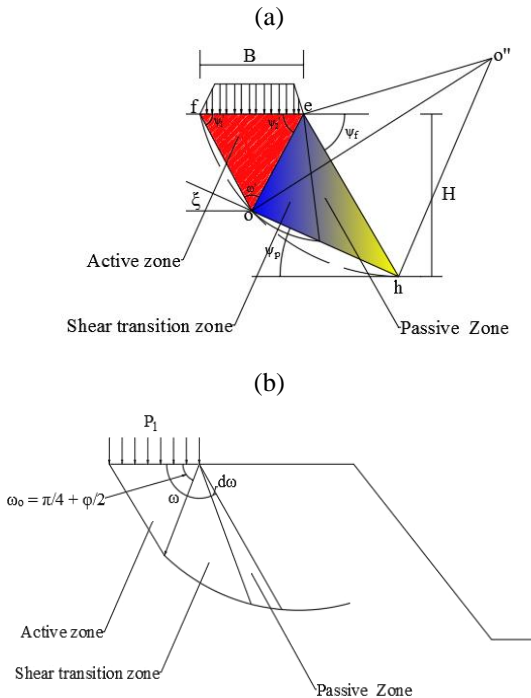


Figure 3. Proposed (a) composite slope stress structure (b) force diagram [29]

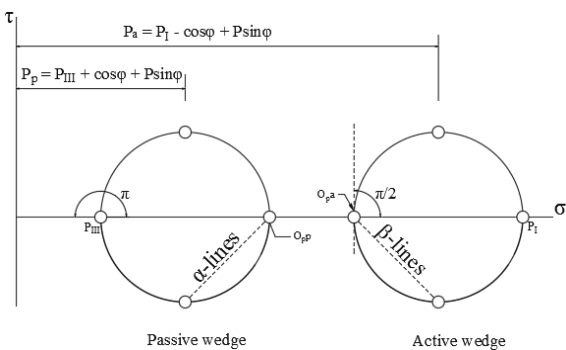


Figure 4. Mohr circle for failure region in active and passive wedges [29]

From the description of α - and β -lines, if the boundary stress happens to be the smaller principal stress, α - and

β -lines make an angle of $\omega_o = \frac{\pi}{4} - \frac{\varphi}{2}$ with the boundary (Fig. 5a). On the other hand if the applied stress from the pressure of the dump happens to be the larger principal stress, the α - and β -lines makes an angle of $\omega = \frac{\pi}{4} + \frac{\varphi}{2}$ with the boundary (Fig. 5b), however the resulting stress states are different.

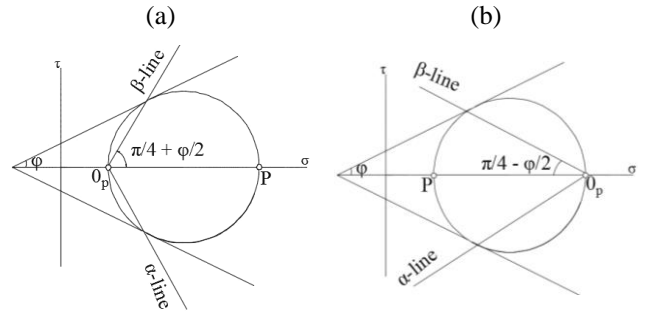


Figure 5. Mohr diagram for an outer dump acting on a half space (active and passive case): (a) active case (I); (b) passive case (III) [29]

The material between the active and passive wedges is filled by a centered fan known as a shear transition zone. The α - and β -lines within the shear transition zone can be deduced by indicating that both lines intersect at an angle of $(\pi/2 - \varphi)$ as indicated in Figure 6 and from the geometry it is evident that $\tan \varphi = dr/rd\omega$ and integrating leads to:

$$\ln\left(\frac{r}{r_o}\right) = (\omega - \omega_o) \tan \varphi. \tag{10}$$

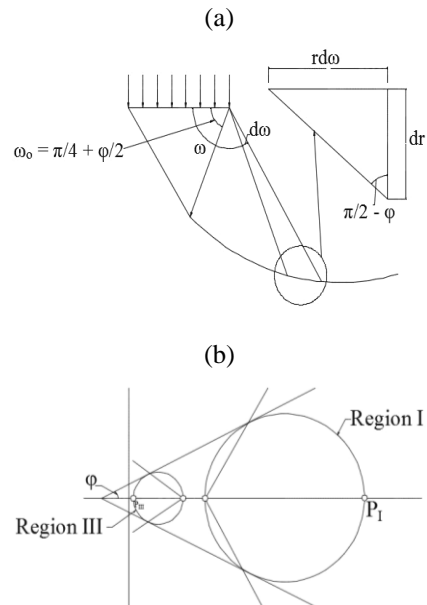


Figure 6. Geometry of slip lines within a centered fan for frictional material [28]

Where r and r_o are defined in Figure 6. Hence all α - and β -lines in the shear transition zones are spiral while α - and β -lines are straight. Considering once again the Mohr circles in Figure 6b, it is seen that the values of ψ in region I and III are $\pi/2$ and π , as both regions are related, lying in the

m -45° line in a $2(\tan \phi)\psi$, $\ln(c + p \tan \phi)$ space. Thus the two-dimensional mean stress p_I and p_{III} must be related by:

$$2(\tan \phi)(\psi_I - \psi_{III}) = -(\tan \phi)\pi = -\ln(c + p_{III} \tan \phi) + \ln(c + p_I \tan \phi). \quad (11)$$

Hence p_I and p_{III} are related to σ_1 and σ_3 by:

$$\sigma_1 = c \cos \phi + p_I (1 + \sin \phi); \quad (12)$$

$$\sigma_3 = -c \cos \phi + p_{III} (1 - \sin \phi). \quad (13)$$

2.2. Triangular loading on an infinite strip based on the theory of elasticity

The stress computational equations for a composite slope due to a waste dump loading based on the principle of superposition [28] is utilized within the theory of plasticity to determine the zone of plastic influence and the induced stresses within a surface mines slope. Figure 7 is a simplified geometry of the composite slope mechanical model which incorporates the basic features and assumption necessary for performing a slope stability analysis under the action of an external load.

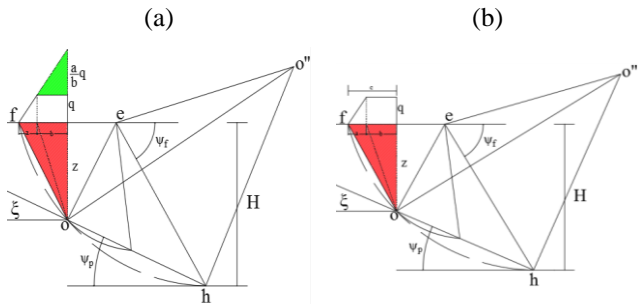


Figure 7. Proposed composite slope stress computation model: (a) slope linearly increasing load structure on composite; (b) half section of a waste dump in a composite slope [28]

The estimation of stress increment at various points along with the associated displacement in a soil mass due to an external load is an important component in the safe design of engineering structures. In many engineering problems, especially those concerning slope stability, stresses imposed and their variation with depths inside the soil mass are of paramount concern. From the theory of elasticity, the stresses due to a vertical line load on the surface can be computed as follows:

$$\sigma_z = \frac{2qz^3}{\pi(x^2 + z^2)^2}; \quad (14)$$

$$\sigma_x = \frac{2qx^2z}{\pi(x^2 + z^2)^2}; \quad (15)$$

$$\tau_{xz} = \frac{2qxz^2}{\pi(x^2 + z^2)^2}. \quad (16)$$

Figure 8 shows a vertical loading on an infinite strip of width $2l$. The load increases from zero to q across the width. For an elementary strip of width dr , the load per unit length can be given as $(q/2l) r \cdot dr$. Approximating this as a line

load, we can substitute $(q/2l) r \cdot dr$ for q and $x - r$ for x in Equation (14) to (16) to determine the stresses at a point (x, z) inside the semi-infinite mass. Thus:

$$\sigma_z = \int d\sigma_z = \left(\frac{1}{2l}\right) \left(\frac{2q}{\pi}\right) \int_{r=0}^{r=2l} \frac{z^3 r dr}{[(x-r)^2 + z^2]^2};$$

$$\sigma_z = \left(\frac{q}{2\pi}\right) \left(\frac{x}{l} \alpha - \sin 2\delta\right); \quad (17)$$

$$\sigma_x = \int d\sigma_x = \left(\frac{1}{2l}\right) \left(\frac{2q}{\pi}\right) \int_{r=0}^{r=2b} \frac{(x-r)^2 z r dr}{[(x-r)^2 + z^2]^2};$$

$$\sigma_x = \left(\frac{q}{2\pi}\right) \left(\frac{x}{l} \alpha - 2.303 \frac{z}{l} \log \frac{R_1^2}{R_2^2} + \sin 2\delta\right); \quad (18)$$

$$\tau_{xz} = \int d\tau_{xz} = \left(\frac{1}{2l}\right) \left(\frac{2q}{\pi}\right) \int_0^{2l} \frac{(x-r)z^2 dr}{[(x-r)^2 + z^2]^2};$$

$$\tau_{xz} = \left(\frac{q}{2\pi}\right) \left(1 + \cos 2\delta - \frac{z}{l} \alpha\right). \quad (19)$$

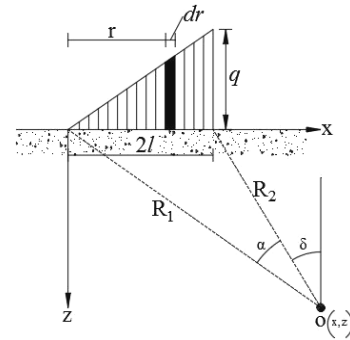


Figure 8. Linearly increasing vertical loading on an infinite strip [28]

2.3. Stresses due to waste dump loading in a semi-infinite mass

In surface mining it is necessary to determine the increase in stress within the soil mass due to the waste dump loading. This can be done by the method of superposition as shown in Figure 9 [28]. The ideal assumption of the theory of elasticity, namely that the medium is homogeneous, elastic and isotropic, is not quite true for most soil profiles, however it does provide a close estimation for computing stresses.

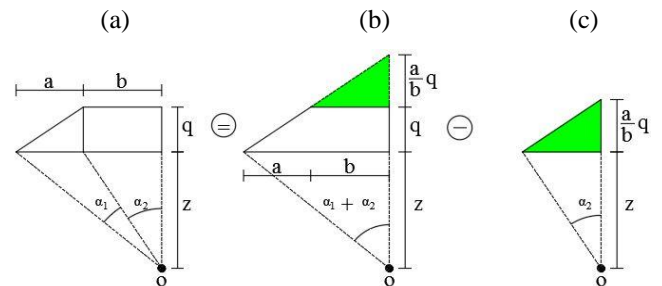


Figure 9. Vertical and horizontal stress computational model due to waste dump loading [28]

2.3.1. Vertical stress component due to waste dump loading in a semi-infinite mass

Referring to Equation (17), the vertical stress component at point O due to the loading shown in Figure 9a can be computed based on the principle of superposition [28], [29]. That is the vertical stress σ_z at O due to the waste dump loading shown in Figure 9a is equal to the stress at O due to the loading shown in Figure 9b minus the stress at O due to the loading shown in Figure 9c. Let $q + (b/a) \cdot q = q$ for the load shown in Figure 9b and $(b/a) \cdot q = q$ for the load shown in Figure 9c then the vertical stress at point O in Figure 9b and Figure 9c can be computed as follows:

$$\sigma_{z(2-9b)} = \left(\frac{q + (b/a)q}{2\pi} \right) \cdot \left(\frac{2l}{l} (\alpha_1 + \alpha_2) \right);$$

$$\sigma_{z(2-9b)} = \frac{q}{\pi} \left(\frac{a+b}{a} \right) \cdot (\alpha_1 + \alpha_2). \quad (20)$$

Similarly, the vertical stress at O due to the loading shown in Figure 9c is:

$$\sigma_{z(2-9c)} = \left(\frac{(b/a) \cdot q}{2\pi} \right) \cdot \left(\frac{2l}{l} \cdot \alpha_2 \right);$$

$$\sigma_{z(2-9c)} = \left(\frac{b}{a} \cdot q \right) \cdot \frac{1}{\pi} \cdot (\alpha_2). \quad (21)$$

Thus the vertical stress at O due to the waste dump loading shown in Figure 9a is:

$$\sigma_z = \sigma_{z(2-9b)} - \sigma_{z(2-9c)}. \quad (22)$$

Substituting (20) and (21) into (22) gives:

$$\sigma_z = \frac{q}{\pi} \left[\left(\frac{a+b}{a} \right) \cdot (\alpha_1 + \alpha_2) - \left(\frac{b}{a} \right) \cdot \alpha_2 \right]. \quad (23)$$

2.3.2. Horizontal stress component due to waste dump loading in a semi-infinite mass

Referring to (18), the horizontal stress component at point O due to the loading shown in Figure 9a can be computed similarly based on the principle of superposition. That is the horizontal stress at O due to the waste dump loading shown in Figure 9a is equal to the stress at O due to the loading shown in Figure 9b minus the stress at O due to the loading shown in Figure 9c. Thus the horizontal stress at point O in Figure 9b and Figure 9c can be computed as follows:

$$\sigma_{x(2-9b)} = \left(\frac{q + (b/a)q}{2\pi} \right) \left[\frac{2l}{l} (\alpha_1 + \alpha_2) - 2.303 \cdot \frac{z}{l} \cdot \log \frac{R_1^2}{R_2^2} \right]; \quad (24)$$

$$\sigma_{x(2-9b)} = \left(\frac{q + (b/a)q}{\pi} \right) \left[(\alpha_1 + \alpha_2) - \frac{2.303}{2} \cdot \frac{z}{l} \cdot \log \frac{R_1^2}{R_2^2} \right]; \quad (25)$$

$$\sigma_{x(2-9b)} = \frac{q}{\pi} \left(\frac{a+b}{a} \right) \left[(\alpha_1 + \alpha_2) - \frac{2.303}{2} \cdot \frac{z}{l} \cdot \log \frac{R_1^2}{R_2^2} \right]. \quad (26)$$

From Figure 9b, $R_1^2 = (a+b)^2 + z^2$ and $R_2^2 = z^2$, hence the value of R_1^2 and R_2^2 can be substituted into (26) such that (26) becomes:

$$\sigma_{x(2-9b)} = \frac{q}{\pi} \left(\frac{a+b}{a} \right) \left[(\alpha_1 + \alpha_2) - \frac{2.303}{2} \cdot \frac{z}{l} \cdot \log \frac{(a+b)^2 + z^2}{z^2} \right]. \quad (27)$$

Since $z \tan(\alpha_1 + \alpha_2) = a + b$ and $a + b = 2l$ then $z = \frac{2l}{\tan(\alpha_1 + \alpha_2)}$; substituting the value of z into (27) and solving for $\sigma_{x(2-9b)}$.

$$\sigma_{x(2-9b)} = \frac{q}{\pi} \left(\frac{a+b}{a} \right) \left[\frac{(\alpha_1 + \alpha_2)}{\frac{2.303}{2} \cdot \frac{2l / \tan(\alpha_1 + \alpha_2)}{l}} \right];$$

$$\sigma_{x(2-9b)} = \frac{q}{\pi} \left(\frac{a+b}{a} \right) \left[\frac{(\alpha_1 + \alpha_2)}{\frac{2.303}{\tan(\alpha_1 + \alpha_2)}} \right]. \quad (28)$$

Similarly, the horizontal stress at O due to the loading shown in Figure 9c is such that:

$$\sigma_{x(2-9c)} = \left(\frac{b}{a} \cdot q \right) \frac{1}{\pi} \left[(\alpha_2) - \frac{2.303}{2} \cdot \frac{z}{l} \cdot \log \frac{R_1^2}{R_2^2} \right]. \quad (29)$$

However, in this case $z = \frac{b}{\tan \alpha_2}$, $2l = b$, $R_1^2 = b^2 + z^2$ and $R_2^2 = z^2$, and substituting these values into (29) gives:

$$\sigma_{x(2-9c)} = \left(\frac{b}{a} \cdot q \right) \frac{1}{\pi} \left[(\alpha_2) - \frac{2.303}{2} \cdot \frac{2b / \tan \alpha_2}{b} \cdot \log \frac{b^2 + z^2}{z^2} \right]; \quad (30)$$

$$\sigma_{x(2-9c)} = \left(\frac{b}{a} \cdot q \right) \frac{1}{\pi} \left[(\alpha_2) - \frac{2.303}{\tan \alpha_2} \cdot \log \frac{b^2 + (b / \tan \alpha_2)^2}{(b / \tan \alpha_2)^2} \right];$$

$$\sigma_{x(2-9c)} = \left(\frac{b}{a} \cdot q \right) \frac{1}{\pi} \left[(\alpha_2) - \frac{2.303}{\tan \alpha_2} \cdot \log(1 + \tan^2 \alpha_2) \right]. \quad (31)$$

Thus the horizontal stress at O due to the waste dump loading shown in Figure 9a is such that:

$$\sigma_x = \sigma_{x(2-9b)} - \sigma_{x(2-9c)}. \quad (32)$$

Substituting the values for $\sigma_{x(2-9b)}$ and $\sigma_{x(2-9c)}$ gives:

$$\sigma_x = \frac{q}{\pi} \left(\frac{a+b}{a} \right) \left[\frac{(\alpha_1 + \alpha_2)}{\frac{2.303}{\tan(\alpha_1 + \alpha_2)} \cdot \log(1 + \tan^2(\alpha_1 + \alpha_2))} \right] - \left(\frac{b}{a} \cdot q \right); \quad (33)$$

$$\frac{1}{\pi} \left[\alpha_2 - \frac{2.303}{\tan \alpha_2} \log(1 + \tan^2 \alpha_2) \right].$$

Factorizing gives,

$$\sigma_x = \frac{q}{\pi} \left[\left(\frac{a+b}{a} \right) \left(\frac{(\alpha_1 + \alpha_2)}{\frac{2.303}{\tan(\alpha_1 + \alpha_2)} \cdot \log(1 + \tan^2(\alpha_1 + \alpha_2))} \right) - \left(\frac{b}{a} \left(\alpha_2 - \frac{2.303}{\tan \alpha_2} \cdot \log(1 + \tan^2 \alpha_2) \right) \right) \right]. \quad (34)$$

2.3.3. Shear stress component due to waste dump loading in a semi-infinite mass

Referring to (19), the shear stress component at point O due to the loading shown in Figure 9a can be computed similarly on the principle of superposition. That is the horizontal stress at O due to the waste dump loading shown in Figure 9a is equal to the shear stress at O due to the loading shown in Figure 9b minus the shear stress at O due to the loading shown in Figure 9c. Thus the horizontal stress at point O in Figure 9b and Figure 9c can be computed as follows:

$$\tau_{xz} = \left(\frac{q}{2\pi}\right)\left(2 - \frac{z}{l}(\alpha_1 + \alpha_2)\right); \quad (35)$$

$$\tau_{xz(2-9b)} = \frac{q}{\pi}\left(\frac{a+b}{a}\right)\left(1 - \frac{z}{2l}(\alpha_1 + \alpha_2)\right). \quad (36)$$

From Figure 3b $z = \frac{2l}{\tan(\alpha_1 + \alpha_2)}$ and substituting the value of z into (23) and solving for $\tau_{xz(2-9b)}$, gives:

$$\tau_{xz(2-9b)} = \frac{q}{\pi}\left(\frac{a+b}{a}\right)\left(1 - \frac{\alpha_1 + \alpha_2}{\tan(\alpha_1 + \alpha_2)}\right). \quad (37)$$

Similarly, the shear stress at O due to the loading shown in Figure 9c is such that:

$$\tau_{xz} = \left(\frac{b}{a}q\right)\frac{1}{2\pi}\left(2 - \frac{z}{l}(\alpha_2)\right);$$

$$\tau_{xz} = \left(\frac{b}{a}q\right)\frac{1}{\pi}\left(1 - \frac{z}{l}(\alpha_2)\right). \quad (38)$$

From Figure 9c $z = \frac{2l}{\tan(\alpha_2)}$ and substituting the value of z into (3)-(38) and solving for $\tau_{xz(2-9c)}$, gives:

$$\tau_{xz} = \left(\frac{b}{a}q\right)\frac{1}{\pi}\left(1 - \frac{\alpha_2}{\tan \alpha_2}\right). \quad (39)$$

Thus the shear stress at O due to the waste dump loading shown in Figure 9a is such that:

$$\tau_{xz} = \tau_{xz(2-9b)} - \tau_{xz(2-9c)}. \quad (40)$$

Substituting the values for $\tau_{xz(2-9b)}$ and $\tau_{xz(2-9c)}$ gives:

$$\tau_{xz} = \left[\frac{q}{\pi}\left(\frac{a+b}{a}\right)\left(1 - \frac{\alpha_1 + \alpha_2}{\tan(\alpha_1 + \alpha_2)}\right) - \left(\frac{b}{a}q\right)\frac{1}{\pi}\left(1 - \frac{\alpha_2}{\tan \alpha_2}\right)\right]. \quad (41)$$

Factoring gives:

$$\tau_{xz} = \frac{q}{\pi}\left[\left(\frac{a+b}{a}\right)\left(1 - \frac{\alpha_1 + \alpha_2}{\tan(\alpha_1 + \alpha_2)}\right) - \left(\frac{b}{a}\right)\left(1 - \frac{\alpha_2}{\tan \alpha_2}\right)\right]. \quad (42)$$

2.4. Effect of the dump position on the stress field of composite slope

Equation (23), (34) and (42) gives the vertical, horizontal and shear stresses beneath a trapezoidal dump based on the theory of elasticity, however according to the plasticity theory the stress generated by rock mass loading, which is transferred from the zone of active pressure (I) to the zone of radial shearing (II) is expressed mathematically as [28][29]:

$$\sigma_1 = c \cos \varphi + P_I (1 + \sin \varphi). \quad (43)$$

While stress generated and transferred from the zone of passive wedge III to zone II is expressed as:

$$\sigma_3 = -c \cos \varphi + P_{III} (1 - \sin \varphi). \quad (44)$$

Substituting (25) and (26) into the mean stress equation:

$$P = \frac{1}{2}(\sigma_{\partial xx} + \sigma_{zz});$$

$$p = \frac{1}{2} \frac{q}{\pi} \left[\frac{2.303}{\tan(\alpha_1 + \alpha_2)} \log(1 + \tan^2(\alpha_1 + \alpha_2)) - \frac{b}{a} \left(2\alpha_2 - \frac{2.303}{\tan \alpha_2} \log(1 + \tan^2 \alpha_2) \right) \right]. \quad (45)$$

Thus, the maximum and minimum stresses induced due to the waste dump loading are as follows:

$$\sigma_1 = c \cos \varphi + \frac{1}{2} \frac{q}{\pi} \left[\frac{2.303}{\tan(\alpha_1 + \alpha_2)} \log(1 + \tan^2(\alpha_1 + \alpha_2)) - \frac{b}{a} \left(2\alpha_2 - \frac{2.303}{\tan \alpha_2} \log(1 + \tan^2 \alpha_2) \right) \right] \times (46)$$

$$\times (1 + \sin \varphi);$$

$$\sigma_3 = -c \cos \varphi + \frac{1}{2} \frac{q}{\pi} \left[\frac{2.303}{\tan(\alpha_1 + \alpha_2)} \log(1 + \tan^2(\alpha_1 + \alpha_2)) - \frac{b}{a} \left(2\alpha_2 - \frac{2.303}{\tan \alpha_2} \log(1 + \tan^2 \alpha_2) \right) \right] \times (47)$$

$$\times (1 - \sin \varphi)$$

From (46) and (47) it is obtained that when the vertical stress $\sigma_1 > \sigma_3$ the ground surface will sink in the z - direction and this occur specifically when the slip line angle $\omega_o = 0$. However, when $\sigma_1 < \sigma_3$, the ground surface will bulge. Equation (25) and (36) represents stresses induced only by the waste dump, thus the principle stress produced by a depth of z is expressed as:

$$\sigma_3 = \left[c \cos \varphi + \frac{1}{2} \frac{q}{\pi} \left[\frac{2.303}{\tan(\alpha_1 + \alpha_2)} \log(1 + \tan^2(\alpha_1 + \alpha_2)) - \frac{b}{a} \left(2\alpha_2 - \frac{2.303}{\tan \alpha_2} \log(1 + \tan^2 \alpha_2) \right) \right] \right] \times (48)$$

$$\times (1 + \sin \varphi) + \gamma H.$$

$$\sigma_3 = \left[c \cos \varphi + \frac{1}{2} \frac{q}{\pi} \left[\begin{aligned} &\left(\frac{a+b}{a} \right) 2(\alpha_1 + \alpha_2) \\ &-\frac{2.303}{\tan(\alpha_1 + \alpha_2)} \log(1 + \tan^2(\alpha_1 + \alpha_2)) \\ &-\frac{b}{a} \left(2\alpha_2 - \frac{2.303}{\tan \alpha_2} \log(1 + \tan^2 \alpha_2) \right) \end{aligned} \right] \right] \times (49)$$

$\times(1 - \sin \varphi)] + \gamma H.$

$$\sigma_3 = \left[-c \cos \varphi + \frac{q}{\pi} \left[\begin{aligned} &\left(\frac{a+b}{a} \right) (\alpha_1 + \alpha_2) \\ &-\frac{2.303}{\tan(\alpha_1 + \alpha_2)} \log(1 + \tan^2(\alpha_1 + \alpha_2)) \\ &-\frac{b}{a} \left(\alpha_2 - \frac{2.303}{\tan \alpha_2} \log(1 + \tan^2 \alpha_2) \right) \end{aligned} \right] \right] \times (50)$$

$\times(1 - \sin \varphi)] + \gamma H.$

Where α_1, α_2, a and b are obtained from Figure 9.

3. Analysis and discussions

3.1. Deformation mechanisms due to progressive loading in surface mining

In order to reveal the stress change during the process of mining, it is essential to know the in-situ stress conditions prior to altering the original ground surface. The numerical modeling software Sigma/W is used to obtain the in-situ stress with in the ground. Sigma/W has a specified analysis type to establish the in-situ stress conditions where the vertical stress is controlled by the specified unit weight and the lateral stress controlled by a specified Poisson's ratio ν or specified K_0 . However, the computed stresses are independent of the specified stiffness E . Hence, to establish the in-situ stress state a unit weight of 20 kN/m^3 and a Poisson's ratio of $\nu = 0.49$ were used in the analysis. In order to reveal the law of stress change in the ground surface, Figure 10a is utilized. Figure 10b shows the results from the numerical analysis of the original ground state. The vertical stresses due to the overburden above the coal seam is relatively easy to be obtained (Fig. 10c), however, sometimes the greatest uncertainty in determining the in-situ stress state lies in the determination of the lateral earth stresses (Fig. 10d).

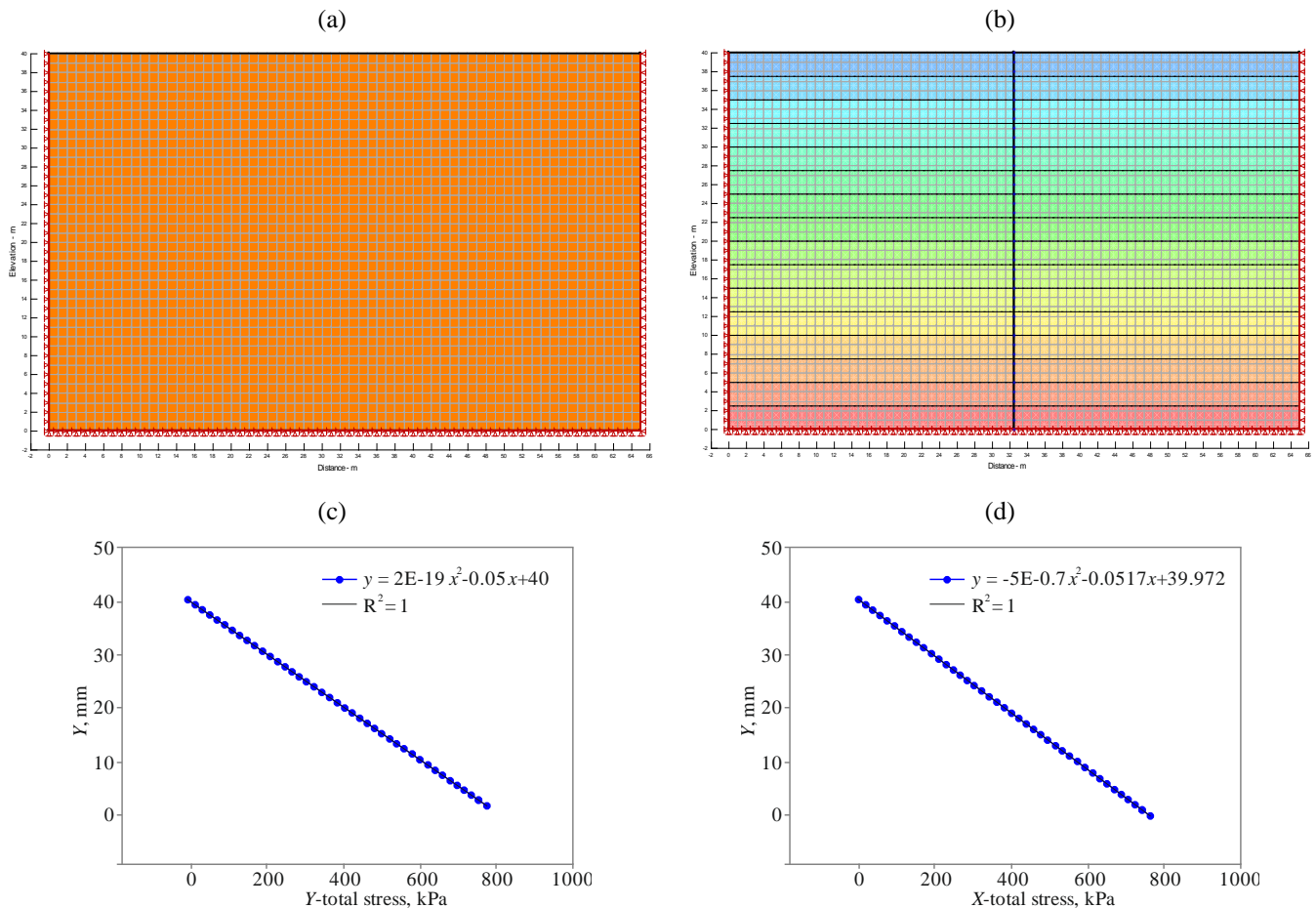


Figure 10. In-situ stress state: (a) original model; (b) graphical output; (c) vertical stress influence rule and (d) horizontal stress influence rule

In order to reveal the law of stress change during the process of excavation, the geometry shown in Figure 11 is utilized. When mining activities occurs, the in-situ stress state within any given surface mines can be changed dramatically. This is because the equilibrium of in-situ stresses is often redistributed and rock masses which

previously contained stresses are removed and the loads are taken elsewhere.

Figure 12a-d shows the numerical results obtained from the analysis. Two separate boundary conditions were simulated to see how the stress behaves in a confined test.

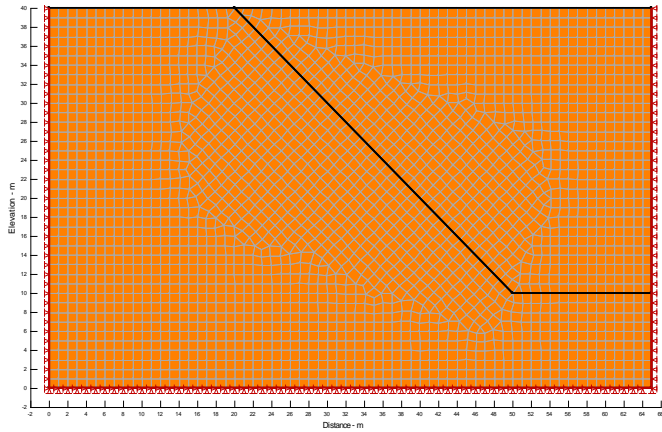


Figure 11. Model used to simulate excavation process in Surface mining

As seen in Figure 12a, the bottom boundary was fixed while rollers were used on the both ends while in Figure 12b the left side had a roller, the bottom fixed but the right-side roller were simulated 10 m above the bottom plane. The reason been when excavating the material above the line forming the slope is removed such that a boundary may not exist within that region as the stress accumulate toward the toe of the slope. Figure 12c-d shows the vertical and horizontal stresses.

3.2. Stress distribution rule of surface mines geometrical parameters

In order to study the effect of the excavation on the induced stress field during the process of mining, the two most critical parameters the slope (height and slope angle) are analyzed using a control variant analysis in Sigma/W. The unit weight and Poisson’s ratio used in the analysis are of the same.

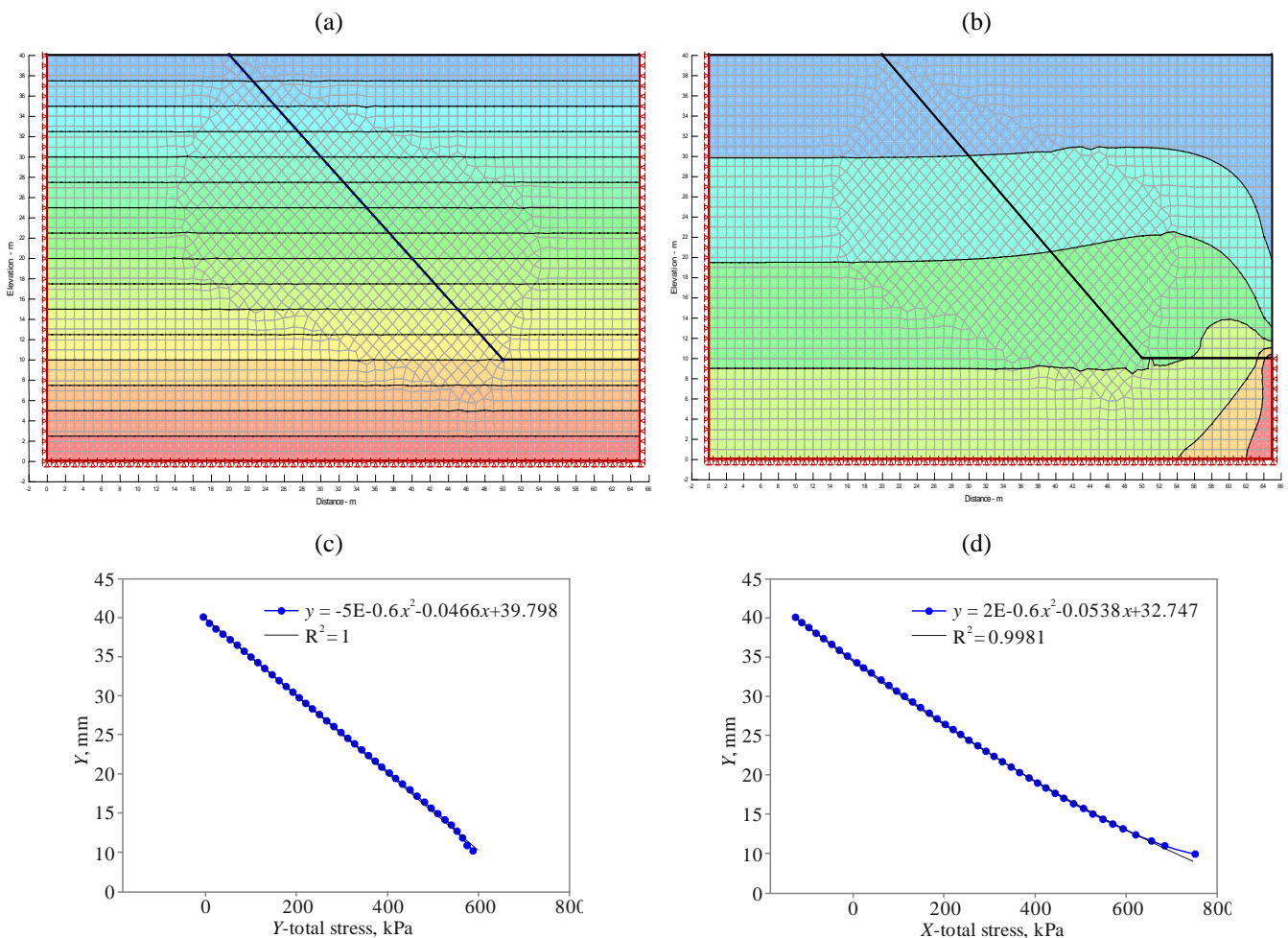


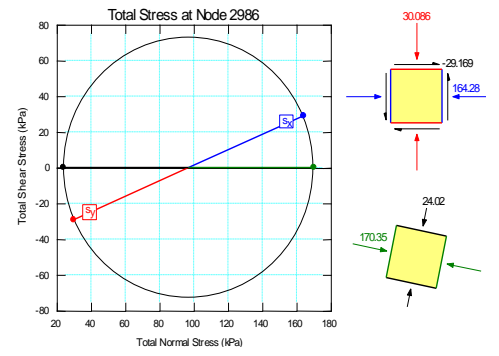
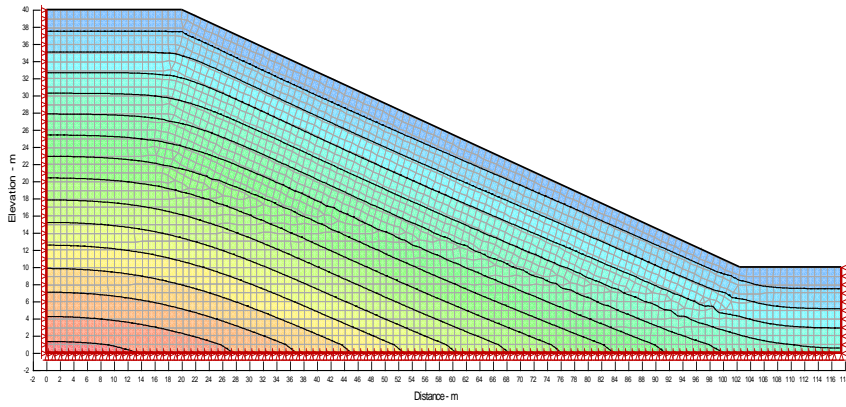
Figure 12. Influence of excavation on the induced stress field: (a) original model; (b) graphical output; (c) vertical stress influence rule and (d) horizontal stress influence rule

3.2.1. Influence of slope angle on the induced stress field

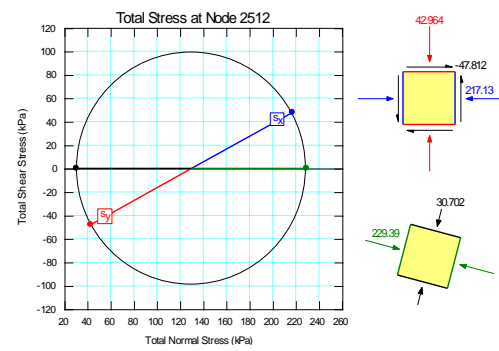
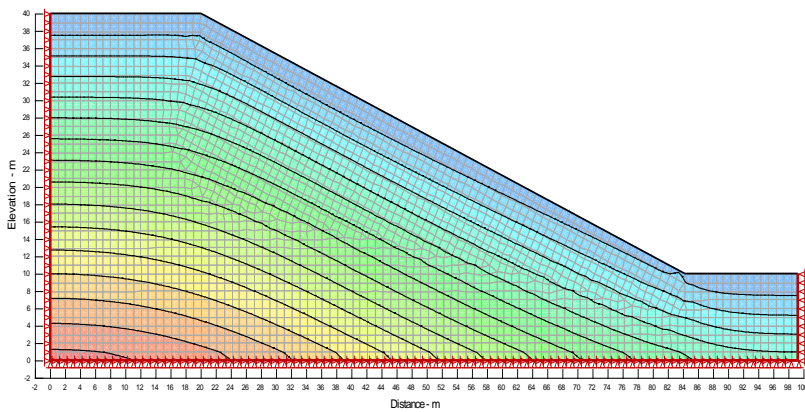
During the open-pit mining process, it is necessary to continuously excavate the overlying rock mass in order to extract the mineral resources. The large-scale mining will cause the redistribution of the stress which would lead to derivation of higher stresses. According to different slope angles in the development of an open pit, the numerical simulation is carried out to reveal the stress development rule by varying the slope angle. The slope angle was vary-

ing from $\psi_f = 20^\circ$ to $\psi_f = 45^\circ$ at 5° interval. Figure 13 shows the graphical output from the numerical simulations of the homogeneous slope. The material properties were constant in all models including the height of the slope. Figure 14a-b shows the vertical and horizontal stress change rule due to variation of the slope angle. The Mohr’s stress diagrams shown in Figure 13 were recorded from the toe of the slope.

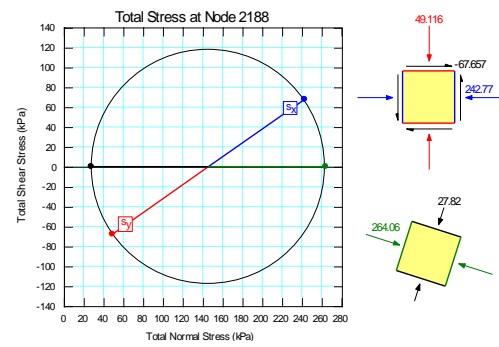
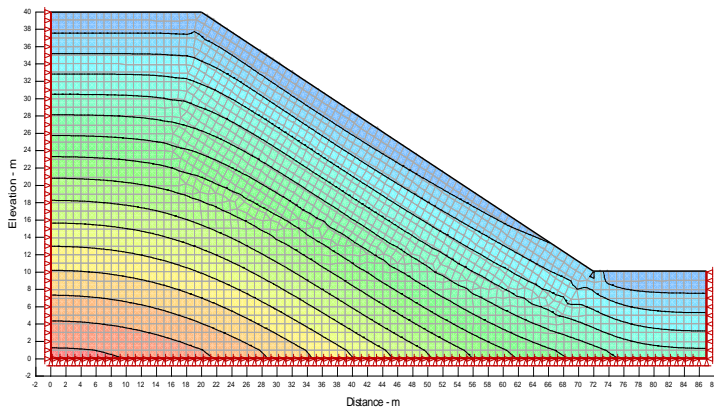
(a)



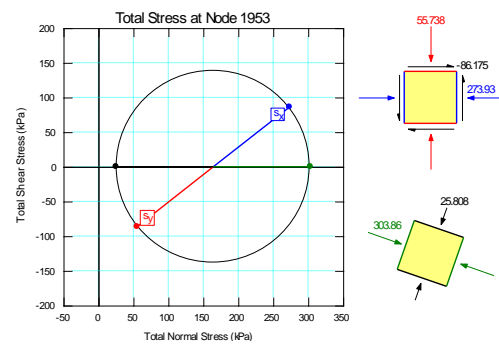
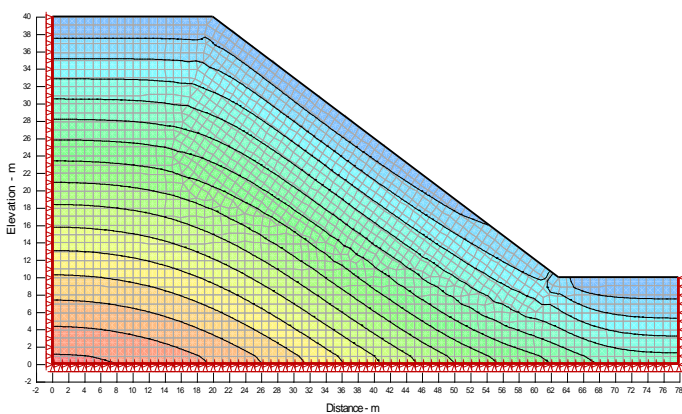
(b)



(c)



(d)



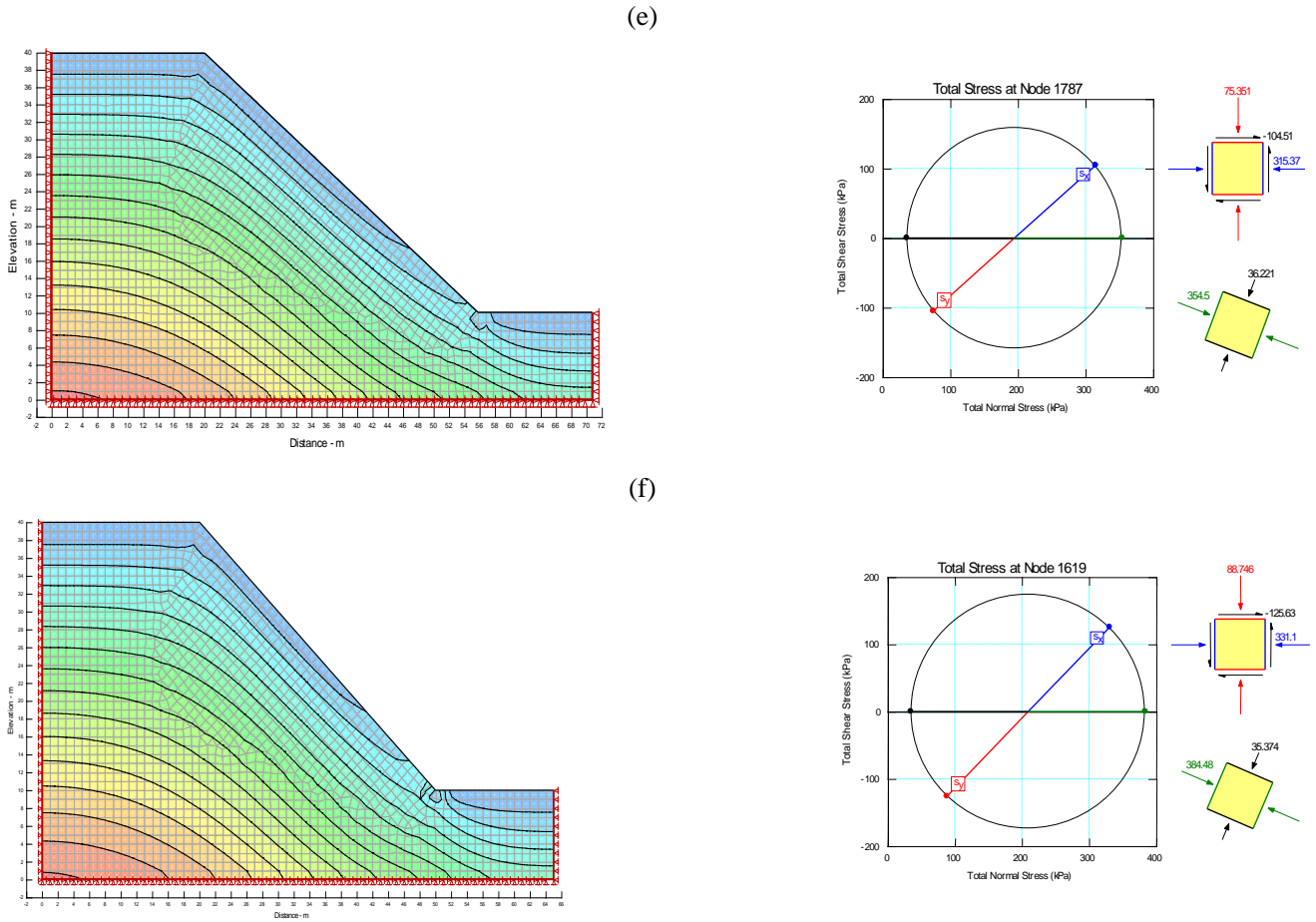


Figure 13. Graphical output of slope angle variation and induced stresses at the toe of the slope: (a) $\psi_f = 20^\circ$; (b) $\psi_f = 25^\circ$; (c) $\psi_f = 30^\circ$; (d) $\psi_f = 35^\circ$; (e) $\psi_f = 40^\circ$; (f) $\psi_f = 45^\circ$

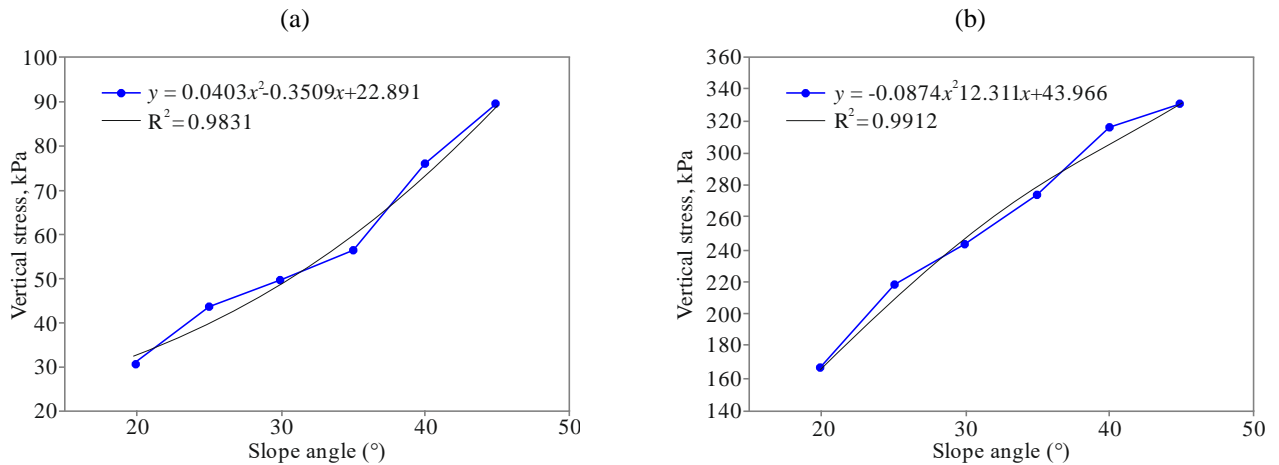


Figure 14. Influence rule of slope angle variation and induced stress at the toe of the slope: (a) vertical stress influence rule; (b) horizontal stress influence rule

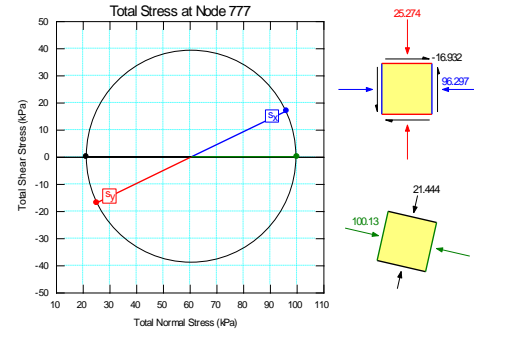
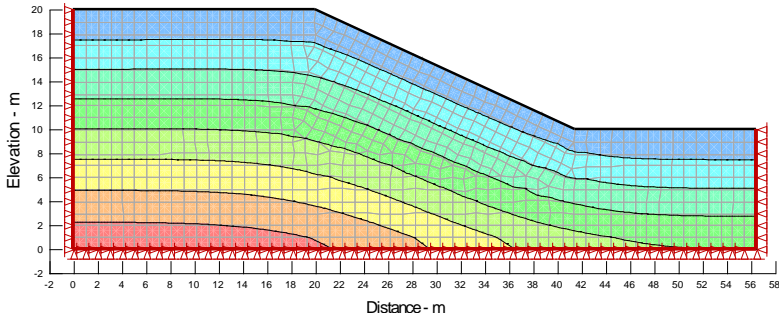
3.2.2. Influence of slope height on the induced stress field

In the mining operation, the rock mass overlying the coal seam is removed in a continuous time-space process in order to extract the mineral resources. According to the development stages of the slope height H in a surface mining operation, the numerical simulation is carried out to reveal the stress development rule. Hence, different slope heights were simulated using Geo slope to reveal the stress development rule by varying the slope height. The

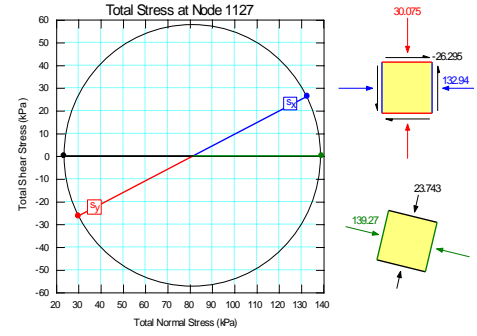
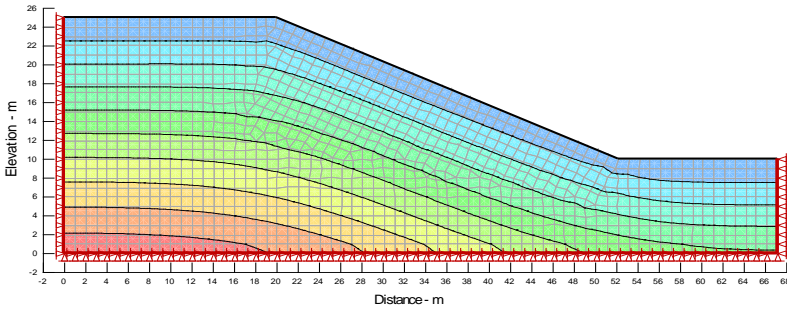
slope height was varying from $H = 10$ m to $H = 40$ m at 5 m interval.

Figure 15 shows the graphical output from the numerical simulations of the homogeneous slope. The material properties were constant in all models including the height of the slope. Figure 16a, b shows the vertical and horizontal stress change rule due to variation of the slope h . The Mohr's stress diagram shown in Figure 15 were recorded from the toe of the slope.

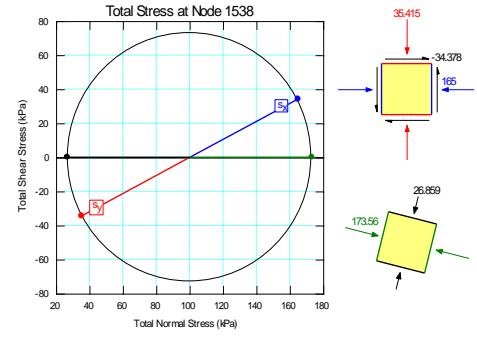
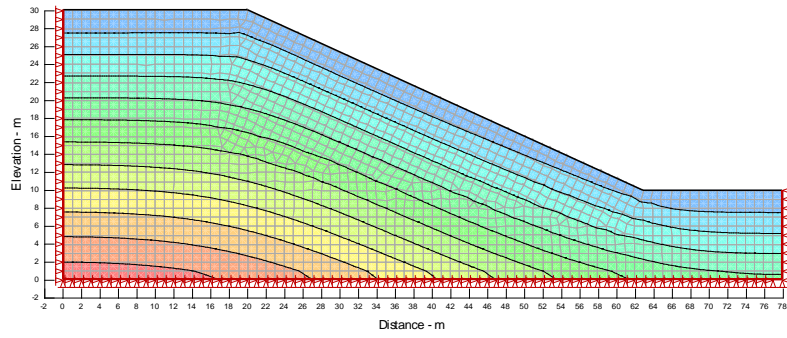
(a)



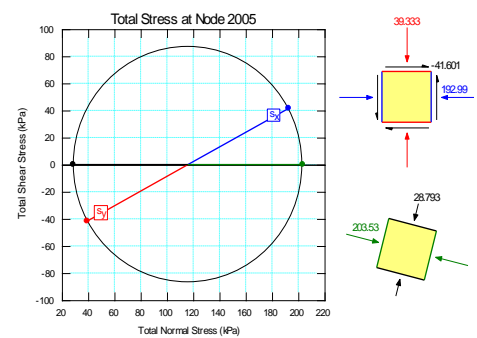
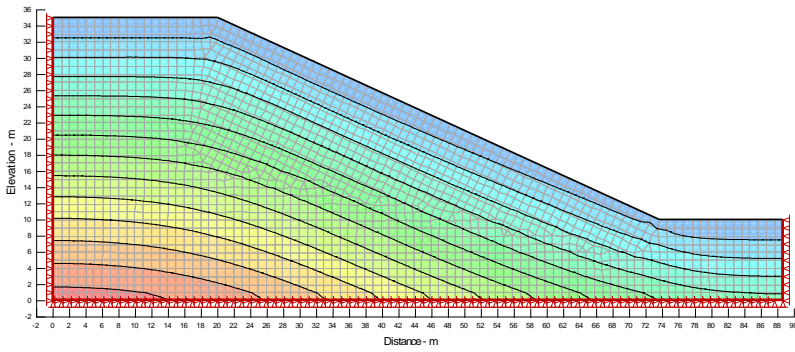
(b)



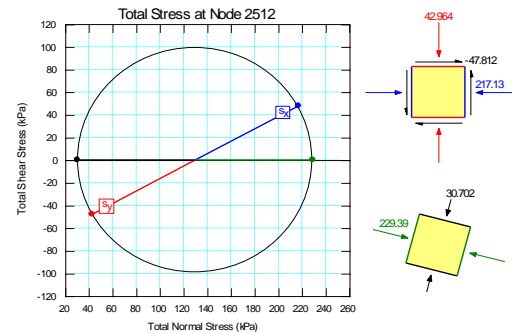
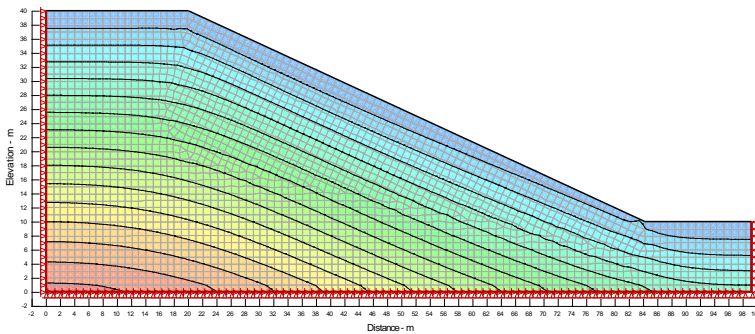
(c)



(d)



(e)



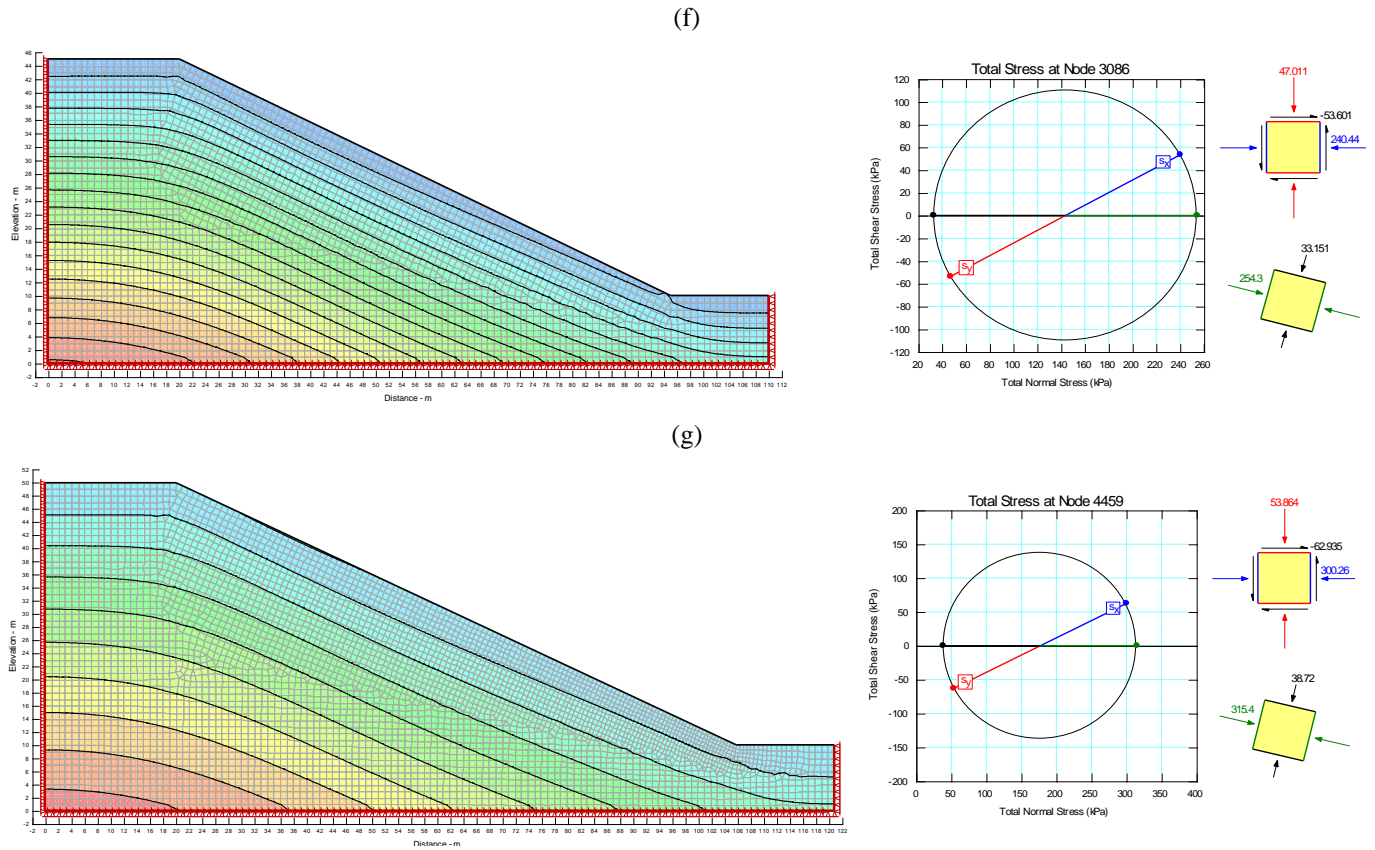


Figure 15. Graphical output of slope height variation and induced stresses at the toe of the slope: (a) $H = 10\text{m}$; (b) $H = 15\text{ m}$; (c) $H = 20\text{ m}$; (d) $H = 25\text{ m}$; (e) $H = 30\text{ m}$; (f) $H = 35\text{ m}$; (g) $H = 40\text{ m}$

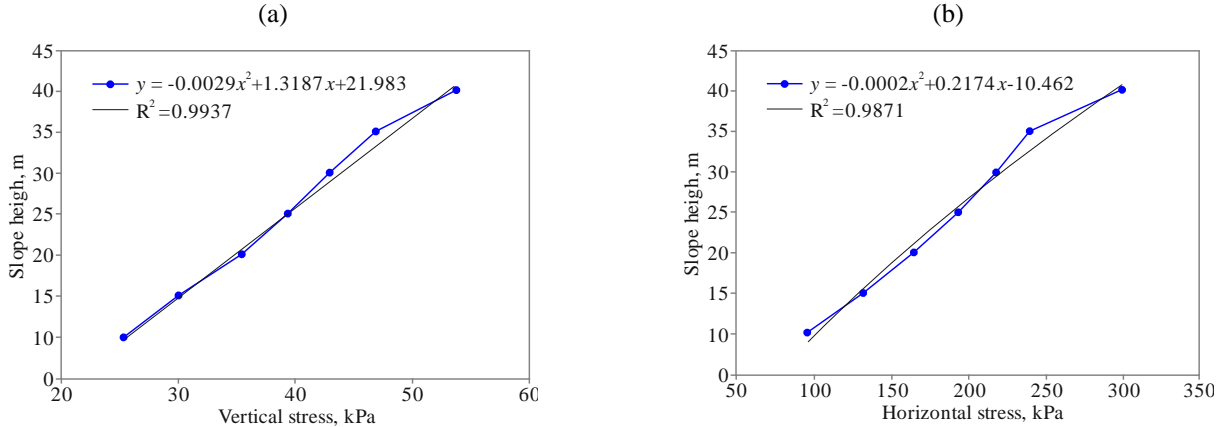


Figure 16. Influence rule of slope height variation and induced stress at the toe of the slope: (a) vertical stress influence rule; (b) horizontal stress influence rule

3.3. Stress variation rule beneath a loaded surface

In order to simulate the change rule due to the dump loading and variation of the dump position, two separate models were simulated using Sigma/W. Since trapezoidal pressure cannot be created in sigma/w the dump pressure is a computed by rearranging the surface area of the dump by using the technique shown in Figure 17. From Figure 17, it can be seen that if the base of the rectangle (x) is known and the base of the triangle ($x_2(\text{m})$), then the trapezoidal surface area can be computed from the rectangle.

From the above analytical formulation, if $x = 10\text{ m}$ and $x_2 = 4.6007\text{ m}$, $H = 5\text{ m}$, the surface area of the trapezoid gives $t_{area} = 38.49825\text{ m}$ while the surface area of the rectangle $r_{area} = 50\text{ m}$. However, a surface area $t_{area} = 3.845\text{ m}$ and

$r_{area} = 5\text{ m}$ were used in the analysis. A pressure of $n = 100\text{ kPa}$ was applied in the model to represent the dump pressure and Figure 18 was used to simulate the effect of the dump loading pressure on a horizontal surface and a sloping ground. Since the focus was to simulate the stresses below the dump, the unit weight of the soil below the dump was set to zero such that the computed stresses represent only those of the dump.

3.3.1. Influence rule of external loading on a horizontal ground surface

Figure 19 shows the graphical output from the numerical simulations of external loading on a semi-infinite mass due to a uniform vertical loading.

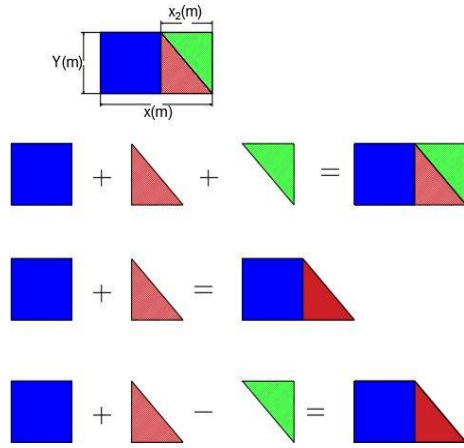


Figure 17. Surface area of trapezoid by rearranging geometrical shapes

Figure 20 shows the results and graphical output from numerical simulation due to a waste dump loading. As seen in Figure 19 and 20, when dump is placed on the surface, the changes in the rock or soil due to the pressure are initiated at the surface of the ground where they show the highest magnitude. The result also shows that the uniform vertical loading induces greater stresses than that of the trapezium load.

3.3.2. Influence rule of external loading on a sloping surface

In order to simulate the influence rule of the dump position on a sloping surface such as that of the surface mines slope, two scenarios were considered. In the first case the dump position was on edge $d =$ on edge while in the second analysis the dump was away from the edge $d >$ on edge.

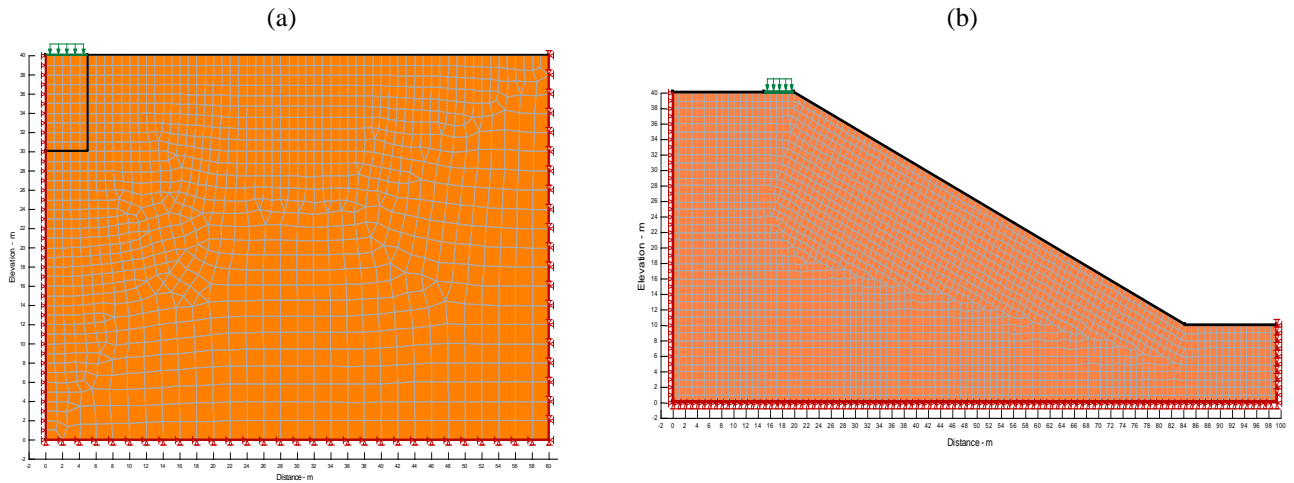


Figure 18. Model used to simulate the effect of dump loading process in surface mining: (a) horizontal ground surface; (b) surface mines slope

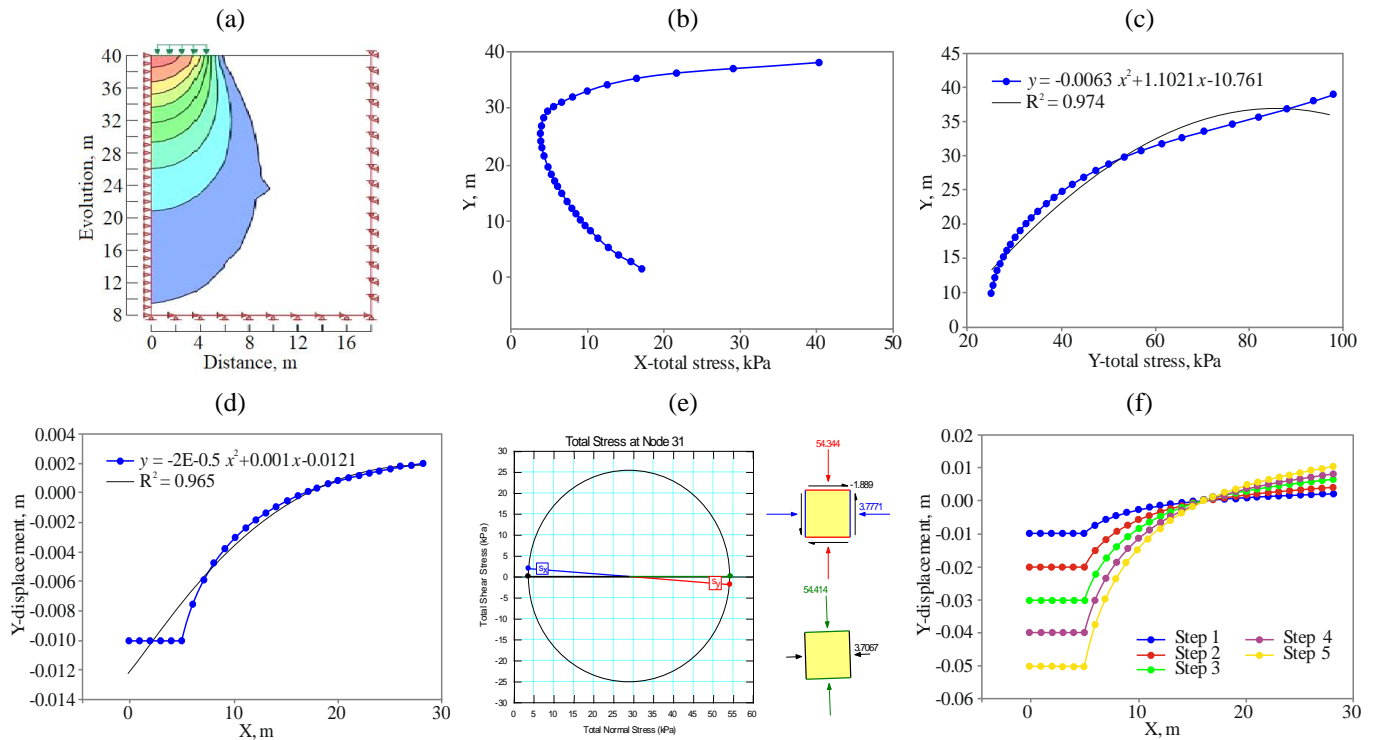


Figure 19. Stress computation due to vertical loading on an infinite strip where $r_{area} = 5$ m: (a) horizontal surface area; (b) pressure bulb beneath the load; (c) vertical stress influence rule; (d) settlement; (e) Mohr's circle; (f) specified incremental loading beneath the loaded area and away from the loaded area

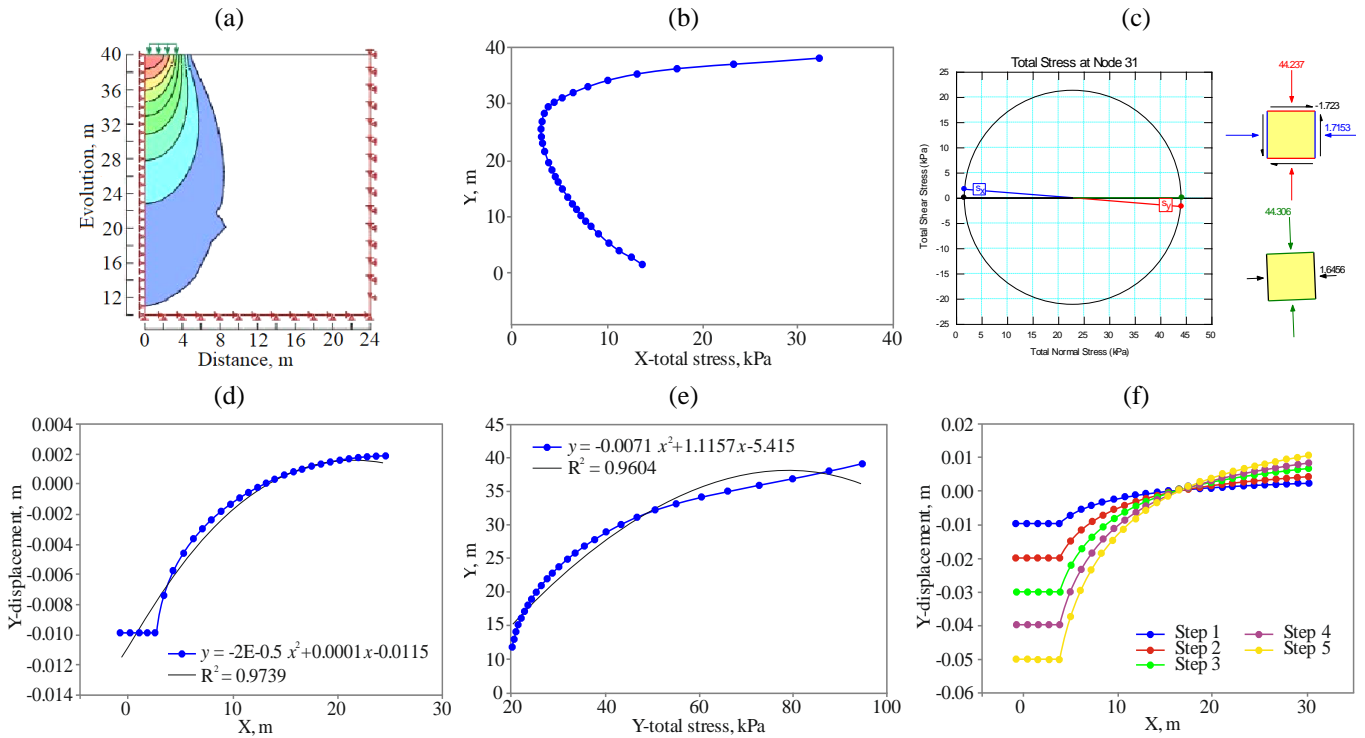


Figure 20. Stress computation due to dump loading on an infinite strip were $t_{area} = 3.845$ m: (a) horizontal surface area; (b) pressure bulb beneath the load; (c) Mohr's circle; (d) vertical stress influence rule; (e) settlement; (f) specified incremental loading beneath the loaded area and away from the loaded area

Figure 21 shows the graphical output from the numerical simulations of external loading on a sloping ground due to loading on edge while Figure 22 shows the graphical output from numerical simulation due to a waste dump loading away from edge. Figure 23 and Figure 24 shows the influ-

ence rule when the dump is on edge and away from the edge of a sloping surface. The results shows that the stresses are greatest beneath the load and diminishes outwardly. Hence it can be seen that as the dump moves away from the point of concentration the induced stresses reduces at that point.

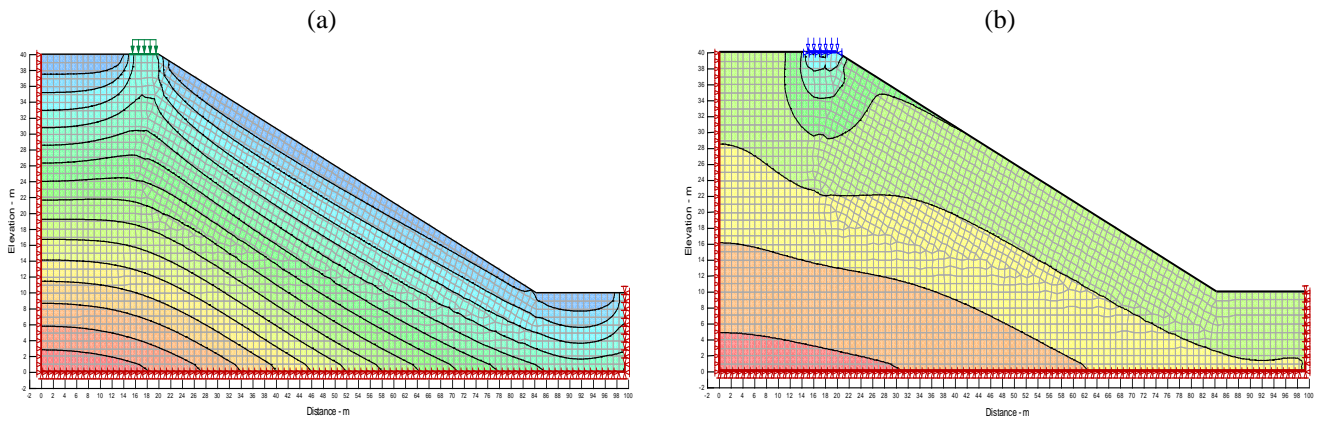


Figure 21. Graphical output of dump loading effect on the induced stresses at the toe of the slope: (a) single load; (b) incremental loading

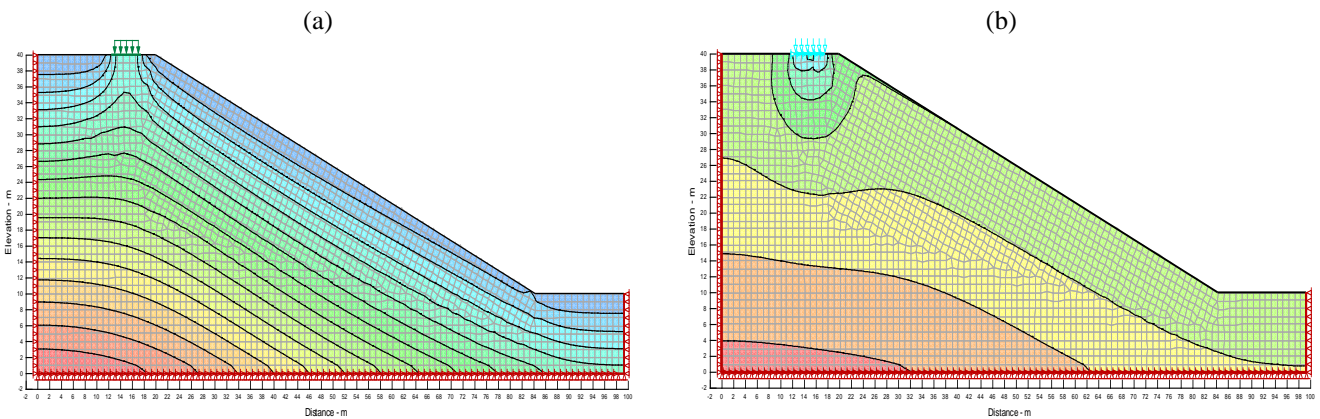


Figure 22. Graphical output of dump loading effect and induced stresses $d >$ on edge: (a) single load; (b) incremental loading

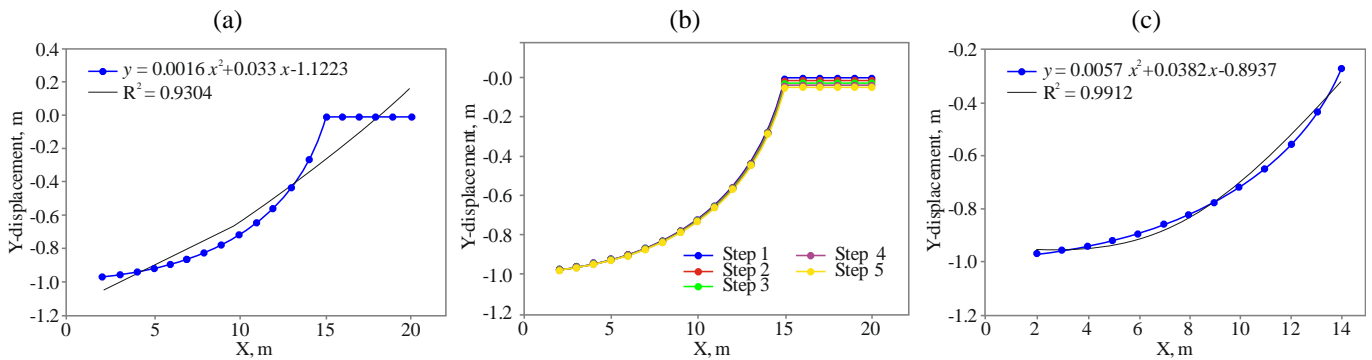


Figure 23. Influence rule of dump loading on the induced $d = \text{on edge}$

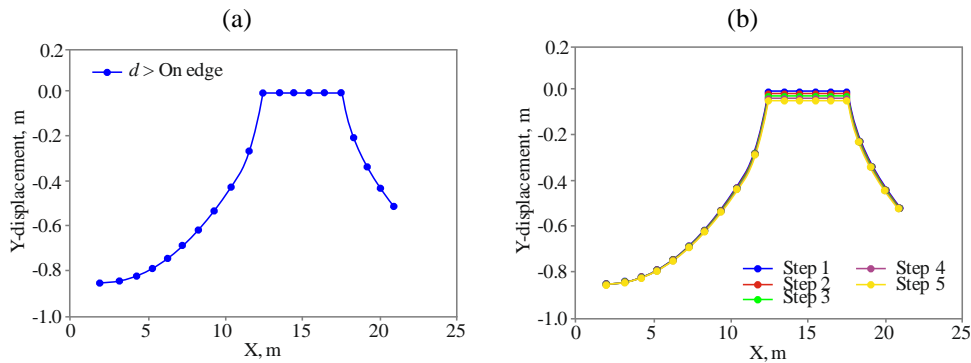


Figure 24. Influence rule of dump loading on the induced $d > \text{on edge}$

4. Conclusions

The simulation results shows that as the height and angle of the slope increases, the stresses of composite slope within the geo field also increases. The stresses are greatest beneath the load and diminish outwardly. Hence it can be seen that as the dump moves away from the point of concentration the induced stresses reduces at that point.

The sensitivity in simulation of waste dump effect is prominent at variable locations in the computational analysis of composite slope. It was noted that the stress induced by trapezoidal loading is less than that of triangular loading

The results also shows that the uniform vertical loading induces greater stresses than that of the trapezium load.

The stress influence rule governed by a surface mining operation is obtained. The stresses due to dump loading obtained and also compared to those obtained from finite element analysis, which are compatible with each other.

Acknowledgments

The authors are thankful to everyone who supported during this research work.

References

[1] Roy, S., & Mandal, N. (2009). Modes of hill-slope failure under overburden loads: Insights from physical and numerical models. *Tectonophysics*, 473(3-4), 324-340. <https://doi.org/10.1016/j.tecto.2009.03.005>

[2] Bonilla-Sierra, V., Elmoultie, M., Donz , F.-V., & Scholt s, L. (2017). Composite wedge failure using photogrammetric measurements and DFN-DEM modelling. *Journal of Rock Mechanics and Geotechnical Engineering*, 9(1), 41-53. <https://doi.org/10.1016/j.jrmge.2016.08.005>

[3] Nunoo, S. (2018). Lessons learnt from open pit wall instabilities: case studies of BC open pit hard rock mines. *Journal of Mining Science*, 54(5), 804-812. <https://doi.org/10.1134/s1062739118054915>

[4] Shruthi, B., Rajurkar, V.J., & Geete, S.S. (2019). Stability analysis of dump slope in open cast mines. *HELIX*, 9(6), 5706-5710. <https://doi.org/10.29042/2019-5706-5710>

[5] Hudson, J.A., & Harrison, J.P. (1997). *Engineering rock mechanics*. Oxford, United Kingdom: Pergamon <https://doi.org/10.1016/b978-008043864-1/50002-1>

[6] Azizi, M.A., Karim, R., Marwanza, I., & Ghifari, M.K. (2019). Prediction of material volume of slope failure in nickel surface mine using limit equilibrium method 3D. *Indonesian Mining Professionals Journal*, 1(1), 43-48. <https://doi.org/10.36986/impj.v1i1.13>

[7] Upadhyay, O.P., Sharma, D.K., & Singh, D.P. (1990). Factors affecting stability of waste dumps in mines. *International Journal of Surface Mining, Reclamation and Environment*, 4(3), 95-99. <https://doi.org/10.1080/09208119008944174>

[8] Nian, T.-K., Huang, R.-Q., Wan, S.-S., & Chen, G.-Q. (2012). Three-dimensional strength-reduction finite element analysis of slopes: geometric effects. *Canadian Geotechnical Journal*, 49(5), 574-588. <https://doi.org/10.1139/t2012-014>

[9] Zaj czkowski, M., Kasztelewicz, Z., & Sikora, M. (2014). Method for location of an external dump in surface mining using the a-star algorithm. *Archives of Mining Sciences*, 59(3), 721-730. <https://doi.org/10.2478/amsc-2014-0050>

[10] Ranjan, V., Sen, P., Kumar, D., & Saraswat, A. (2016). Enhancement of mechanical stability of waste dump slope through establishing vegetation in a surface iron ore mine. *Environmental Earth Sciences*, 76(1). <https://doi.org/10.1007/s12665-016-6350-6>

[11] Singh, A.P., & Singh, T.N. (2006) Assessing instability of coal mine waste dump. *The Indian Mineral Industry Journal*, 113-118.

[12] Steiakakis, E., Kavouridis, K., & Monopolis, D. (2009). Large scale failure of the external waste dump at the "South Field" lignite mine, Northern Greece. *Engineering Geology*, 104(3-4), 269-279. <https://doi.org/10.1016/j.enggeo.2008.11.008>

[13] Jiang, H.B., Hu, T., Li, S.C., & Li, J. (2011). Dump slope stability analysis and landslide forecast research. *Applied Mechanics and Materials*, (71-78), 4642-4644. <https://doi.org/10.4028/www.scientific.net/amm.71-78.4642>

[14] Singh, T.N., & Chaulya, S.K. (1992). External dumping of overburden in opencast mine. *Indian Journal of Engineers*, 22(1 & 2), 65-73.

[15] Singh, T.N., Singh, A.P., & Goyal, M. (1994). Stability of waste dump and its relation to environment. *Indian Journal of Cement Review*, 9(2), 15-21.

[16] Landva, A., & Knowles, G.D. (1990). *Geotechnics of waste fills: theory and practice*. Philadelphia, United States: ASTM.

[17] Ugai, K. (1989). A method of calculation of total safety factor of slope by elasto-plastic FEM. *Soils and Foundations*, 29(2), 190-195. https://doi.org/10.3208/sandf1972.29.2_190

[18] Chaney, R., Demars, K., Pelkey, S., Valsangkar, A., & Landva, A. (2001). Shear displacement dependent strength of municipal solid

- waste and its major constituent. *Geotechnical Testing Journal*, 24(4), 381. <https://doi.org/10.1520/gtj11135j>
- [19] McCarter, M.K. (1990). Design and operating considerations for mine waste embankments. In *Surface Mining* (pp. 890-899). Littleton, United States: Society for Mining, Metallurgy and Exploration.
- [20] Campbell, D.B. (1992). Resloping of waste rock dumps. *International Mine Waste Management News*, 2(2), 7-10.
- [21] Kocasoy, G., & Curi, K. (1995). The ümraniye-hekimbaşı open dump accident. *Waste Management & Research*, 13(4), 305-314. <https://doi.org/10.1177/0734242x9501300402>
- [22] Blight, G. (2008). Slope failures in municipal solid waste dumps and landfills: a review. *Waste Management & Research*, 26(5), 448-463. <https://doi.org/10.1177/0734242x07087975>
- [23] Huang, M., & Li, X. (2007). *Analysis of stability of waste-dump slope of a mine*. Athens, Greece: School of Mining and Metallurgical Engineering.
- [24] Huvaj-Sarihan, N., & Stark, T.D. (2008). Back analyses of landfill slope failures. *Proceedings of 6th International Case Histories Conference*, 11-16.
- [25] Naghadehi, M.Z., Jimenez, R., KhaloKakaie, R., & Jalali, S.-M.E. (2011). A probabilistic systems methodology to analyze the importance of factors affecting the stability of rock slopes. *Engineering Geology*, 118(3-4), 82-92. <https://doi.org/10.1016/j.enggeo.2011.01.003>
- [26] Kainthola, A., Verma, D., Gupte, S.S., & Singh, T.N. (2011). A coal mine dump stability analysis – a case study. *Geomaterials*, 01(01), 1-13. <https://doi.org/10.4236/gm.2011.11001>
- [27] Geoslope.com. (2019). *GEOSLOPE Home*. [online]. Available at: <https://www.geoslope.com>
- [28] Csuohio.edu. (2016). *Academic Server*. Cleveland State University. [online]. Available at: <https://academic.csuohio.edu>
- [29] Ox.ac.uk. (2013). *A.B. Zavatsky*. [online]. Available at: <http://users.ox.ac.uk/~kneabz>

Механізми деформації та розподіл напружень у композитних укосах кар'єрів

Я.Й. Барвор, Ш. Бача, Ц. Кінгхіанг, Ч.С. Жао, М. Сіддікуе

Мета. Дослідження механізмів деформації і розподілу напружень в композитних укосах кар'єрів за допомогою чисельного моделювання методом скінчених елементів для прогнозу їх стійкості.

Методика. Опис та інтерпретація механічної розрахункової моделі напружень для відвалу порожньої породи в процесі формування композитного укосу виконано на основі теорії пластичності та пружності. Проведено чисельне й аналітичне моделювання розподілу напружень в композитному схилі за допомогою використання потужного програмного забезпечення Sigma/W, який функціонує на основі методу скінчених елементів.

Результати. Чисельне та аналітичне моделювання дозволило встановити, що збільшення висоти і кута укосу призводить до збільшення напружень в геонапруженому полі композитного укосу. Чисельне моделювання також показало, що в міру відсування відвалу від точки прикладання навантаження, викликане ним осідання породи в більшій мірі проявляється під відвалом і зменшується при віддаленні від нього, що призводить до зменшення напружень. Дана тенденція показує чутливість моделі, яка описує вплив відвалу в різних точках при чисельному аналізі стійкості композитного укосу. Встановлено, що напруження, викликане трапецевидним навантаженням, менше, ніж напруження, що виникає під дією прямокутного навантаження. Сформульовано принципи впливу напружень, що виникають при відкритій розробці родовищ. Напруження, викликані навантаженням відвалу, були проаналізовані у порівнянні з напруженнями, одержаними за допомогою аналізу скінчених елементів, при цьому результати в обох випадках добре узгоджувалися між собою.

Наукова новизна. Запропоновано новий підхід до аналізу механізмів розподілу напружень в композитному укосі та механізмів деформації. Зв'язок між умовами навантаження і параметрами укосу аналізується за допомогою теорії пластичності та пружності.

Практична значимість. Результати дослідження ефективно описують механізми розподілу напружень і дозволяють проаналізувати стійкість композитних укосів, що є основою для попереднього проектування стійкого композитного укосу.

Ключові слова: композитний укос, механізм деформації, відвал порожньої породи, теорія пластичності, метод скінчених елементів

Механизмы деформации и распределение напряжений в композитных откосах карьеров

Я.Й. Барвор, Ш. Бача, Ц. Кингхианг, Ч.С. Жао, М. Сиддикуе

Цель. Исследование механизмов деформаций и распределения напряжений в композитных откосах карьеров при помощи численного моделирования методом конечных элементов для прогноза их устойчивости.

Методика. Описание и интерпретация механической расчетной модели напряжений для отвала пустой породы в процессе формирования композитного откоса выполнено на основе теории пластичности и упругости. Проведено численное и аналитическое моделирование распределения напряжений в композитном откосе посредством использования мощного программного обеспечения Sigma/W, функционирующего на основе метода конечных элементов.

Результаты. Численное и аналитическое моделирование позволило установить, что увеличение высоты и угла откоса приводит к увеличению напряжений в геонапряженном поле композитного откоса. Численное моделирование также показало, что по мере отодвижения отвала от точки приложения нагрузки, вызванная им осадка породы в большей степени проявляется под отвалом и уменьшается при удалении от него, что приводит к уменьшению напряжений. Данная тенденция показывает чувствительность модели, описывающей влияние отвала в разных точках при численном анализе устойчивости композитного откоса. Установлено, что напряжение, вызванное трапецидальной нагрузкой, меньше, чем напряжение, возникающее под действием прямоугольной нагрузки. Сформулированы принципы влияния напряжений, возникающих при открытой разработке месторождений. Напряжения, вызванные нагрузкой отвала, были проанализированы в сравнении с напряжениями, полученными с помощью анализа конечных элементов, при этом результаты в обоих случаях хорошо согласовывались друг с другом.

Научная новизна. В статье предложен новый подход к анализу механизмов распределения напряжений в композитном откосе и механизмов деформации. Связь между условиями нагружения и параметрами откоса анализируется с помощью теории пластичности и упругости.

Практическая значимость. Результаты исследования эффективно описывают механизмы распределения напряжений и позволяют проанализировать устойчивость композитных откосов, что является основой для предварительного проектирования устойчивого композитного откоса.

Ключевые слова: композитный откос, механизм деформации, отвал пустой породы, теория пластичности, метод конечных элементов

Article info

Received: 5 March 2020

Accepted: 16 October 2020

Available online: 7 November 2020